Journal of Power Sources 239 (2013) 415–423

Contents lists available at SciVerse ScienceDirect

Journal of Power Sources

journal homepage: www.elsevier.com/locate/jpowsour

Electrocatalyst synthesized from metal organic frameworks

Foroughazam Afsahi, Hoang Vinh-Thang, Serguei Mikhailenko, Serge Kaliaguine*

Department of Chemical Engineering, Laval University, Québec, Canada G1V 0A6

HIGHLIGHTS

- Pt-based MOF is synthesized as a novel precursor to prepare PEMFCs electrocatalysts.
- The material is pyrolyzed to form a carbon support and provide electron conductivity.
- The most promising electrocatalyst exhibited power density of 0.58 W mg_{Pt}^{-1}.

GRAPHICAL ABSTRACT

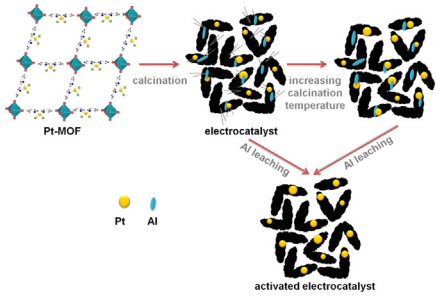

ARTICLE INFO

Article history:
Received 20 December 2012
Received in revised form
12 March 2013
Accepted 27 March 2013
Available online 9 April 2013

Keywords:
PEMFC
Electrocatalyst
MOF
Platinum nanoparticles
Polarization curve
Fitting equation

ABSTRACT

Pt nanoparticles as the common electrocatalyst for proton exchange membrane fuel cells (PEMFCs) were prepared for the first time from metal organic frameworks (MOFs). Pt containing MOF was synthesized and subsequently subjected to pyrolytic carbonization under non-reactive gas atmosphere. Upon pyrolysis, Pt nanoparticles embedded in electronically conductive carbon media were produced. The as-synthesized MOF materials and the prepared electrocatalysts were characterized by XRD, N_2 physisorption, TEM and XPS. The Pt dispersion of obtained electrocatalysts was determined by hydrogen chemisorption. Their conductivity was measured by impedance spectroscopy. The membrane-electrode assemblies (MEAs) made of these electrocatalysts were tested as both anode and cathode in a H_2/air single cell fuel cell. As the anode, the most promising electrocatalyst (C_3) demonstrated an open circuit voltage of 970 mV and power density of 0.58 W mg_{Pt}^{-1} comparable to the commercial electrode power density (0.64 W mg_{Pt}^{-1}) at 0.6 V in a single cell test. At the cathode, a power density of 0.38 W mg_{Pt}^{-1} at 0.6 V was achieved. This confirms the promising potential of this simple approach to be used as a technique to prepare efficient fuel cell electrocatalysts.

1. Introduction

Proton exchange membrane fuel cells (PEMFCs) operated on hydrogen fuel and air (or oxygen), are considered as promising electrical power sources. Unlike internal combustion engines, PEMFCs provide high energy conversion efficiency at relatively low operating temperatures with zero or low greenhouse gas emissions [1,2]. In spite of these advantages, the high cost of PEMFCs mostly related to platinum (Pt)-based electrocatalysts strongly impedes their large-scale commercialization [3,4].

Extensive efforts toward developing effective non-platinum group metal (non-PGM) catalysts during past decades have failed to provide both high activity comparable to Pt and long-term stability under practical fuel cell operating conditions. Therefore, Pt or Pt alloys are remaining as the only realistic choice at least until some phenomenal innovation happens in the development of these materials [5–7]. In this context, it is vital to develop appropriate strategies to reduce Pt content and maximize Pt utilization in the electrodes.

* Corresponding author. Tel.: +1 418 656 2708; fax: +1 418 656 3810.
E-mail address: serge.kaliaguine@gch.ulaval.ca (S. Kaliaguine).

0378-7753/$ – see front matter © 2013 Elsevier B.V. All rights reserved.
http://dx.doi.org/10.1016/j.jpowsour.2013.03.164

Pt nanoparticles ranging from 2 to 3 nm in size supported on carbon black (CB) with high specific surface area represent the most widely used catalyst material for PEMFC. Apart from the particle size, a significant role in catalytic activity of metal nanoparticles is played by the particle shape [8] and the structural features of a catalyst support [9].

In order to minimize the Pt loading and maximize its utilization, while reaching high catalytic activity, numerous synthetic approaches have been attempted. Most of these techniques involve first the formation of a conductive and porous carbon support followed by deposition of Pt onto the support. Pt deposition is most commonly performed by wet chemical method (impregnation with a soluble salt followed by reduction) [10]. Other methods such as atomic layer deposition [11], vacuum deposition [12], etc., have been used less frequently. All these methods have some limitations regarding effective Pt dispersion and therefore do not allow maximum catalyst utilization to be achieved. They mainly bring about the metal particles, distributed in a stochastic manner on the surface of carbon support with sizes higher or at best equal to 2 nm. The broad size distribution of the catalyst particles along with randomness of their spatial scattering are the main obstacles toward developing efficient catalysts with a regular structure and controlled properties.

In the present study, a Pt-based metal organic framework (MOF) is synthesized and applied as a novel precursor for preparing PEMFC electrocatalyst. The synthesized material is subsequently pyrolyzed to form a carbon based support and provide electronic conductivity. MOF materials as the name suggests, are frameworks comprised of metal ions or metal ion clusters linked together by bifunctional organic ligands [13,14]. These highly crystalline structures possess a set of unique characteristics, such as high specific surface area, various pore sizes and geometry, and diverse surface composition, which leads to extensive investigations toward many important applications such as gas storage [15–17], gas separation [18–22], drug delivery [23–25], and catalysis [26–28]. Furthermore, MOF materials have been used as a template and/or carbon source to synthesize nanoporous carbon (NPC) materials with high specific surface area [29–31].

The application of MOFs as electrocatalyst in fuel cell is a quite novel approach. Zeolitic imidazolate frameworks (ZIFs) as a subclass of MOFs have been investigated as precursors for non-PGM electrocatalysts [32–34]. Co [32] and Fe [34] imidazolate frameworks, in which each metal atom is coordinated with four nitrogen atoms of imidazolate ligands to form Co (or Fe)N_4 moieties regularly dispersed in the framework, are used as ORR catalyst precursors. However, the catalytic performances of these materials in PEMFCs are not reported. In another approach [33], ZIF-8 (Zn(II) zeolitic imidazolate framework), with a high nitrogen content and high microporous surface area, is used as the host for Fe and N precursors for preparing PEMFCs catalysts. The highest volumetric activity of 230 A cm^{-3} at 0.8 $V_{iR\text{-}free}$, reported to date is measured for non-PGM-based ORR catalysts in PEMFCs. In this work, we report for the first time a Pt-based MOF material as a precursor to prepare PEMFC electrocatalysts. MOFs have clearly-defined three-dimensional crystalline structures in which metal species are distributed evenly through the crystal. Using Pt containing MOFs as a precursor is expected to provide the high and uniform dispersion of active sites required for an ideal performance of PEMFC electrocatalyst. In addition, the organic linkers can be carbonized via pyrolysis, while maintaining the porous framework, leading to catalysts with high surface area and uniformly distributed active sites. Carbonization will also provide electron conductive media. Therefore, there will be no need for a preformed carbon support which is an essential part of traditional FC electrocatalysts.

2. Experimental

2.1. Synthesis of Pt-based MOF

Pt-based MOF-253 materials as the electrocatalyst precursor were synthesized in two steps according to the reported procedure [35]. To synthesize MOF-253 (first step), 0.625 mmol (151 mg) of $AlCl_3 \cdot 6H_2O$ was dissolved in DMF (10 mL), followed by the addition of 0.625 mmol (153 mg) of 2,2′-bipyridine-5,5′-dicarboxylic acid (bpydc) (Fig. 1a). The obtained mixture was then placed in a Teflon-capped vial and heated at 120 °C for 24 h. The resulting white microcrystalline powder was then filtered and washed with DMF. To obtain fully desolvated framework, this powder was subsequently washed with methanol via soxhlet extraction for 24 h, then collected by filtration and finally dried at 180 °C under dynamic vacuum for 12 h. In order to introduce Pt atoms (second step),

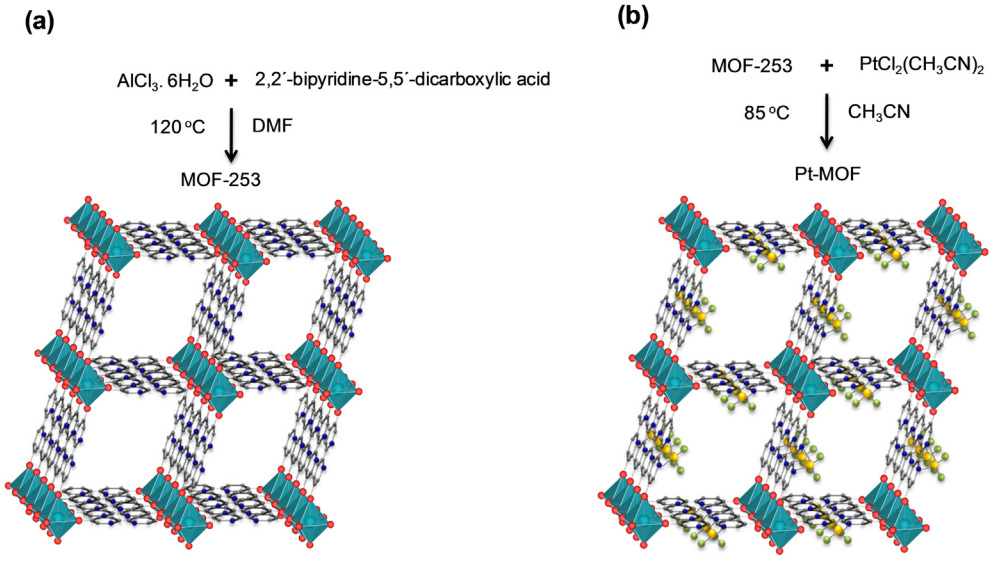

Fig. 1. Synthesis and structure of Pt-MOF. Al atoms (cyan octahedra), yellow, green, red, blue, and gray spheres stand for Pt, Cl, O, N, and C atoms, respectively; H atoms are omitted for simplicity. (For interpretation of the references to color in this figure legend, the reader is referred to the web version of this article.)

1.75 mmol (500 mg) of the desolvated MOF-253 was mixed with 1.11 mmol (386 mg) of $PtCl_2(CH_3CN)_2$ and acetonitrile (15 mL) (Fig. 1b). This mixture was then heated at 85 °C in a Teflon-capped vial for 72 h. The resulting solid was collected by filtration and immersed in acetonitrile (15 mL). The total immersion time was three days and the solvent was replaced with fresh acetonitrile after each 24 h. Finally, the product (hereafter referred to as Pt-MOF) was collected by filtration and dried at 150 °C for 12 h under vacuum.

2.2. Pyrolytic transformation of the Pt-based MOF into electrocatalysts

To prepare the PEMFC electrocatalysts, the Pt-MOF materials were heat treated at temperatures ranging between 700 and 1050 °C. A quartz tube (6 mm diameter) containing 150 mg of the sample was weighed and placed inside a furnace. The tube was sealed airtight and then purged with argon for 1 h prior to the treatment. The materials were typically heated at the ramp rate of 1 °C min^{-1} for 4 h under flow of argon at a rate of 20 mL min^{-1}. The yield after the heat treatment was normally about 50 wt%. A set of four batches of electrocatalyst were prepared, which were designated as C_1–C_4 for samples pyrolyzed at 700, 800, 950 and 1050 °C, respectively.

2.3. Characterization of the synthesized Pt-MOF and electrocatalysts

The phase identification and crystallinity of the synthesized Pt-MOF and the prepared electrocatalysts were determined by X-ray diffraction (XRD) using a SIEMENS D5000 diffractometer with Cu Kα radiation ($\lambda = 0.15406$ nm). Phase recognition was obtained by comparison to Joint Committee on Powder Diffraction Standards (JCPDS) files. The specific surface areas of the Pt-MOF and C_1–C_4 electrocatalysts were established by Brunauer–Emmett–Teller (BET) analysis of the nitrogen adsorption–desorption isotherms recorded at −196 °C using a Quantachrome instrument. All the samples were degassed by heating at 150 °C under vacuum prior to measuring the surface area. The BET specific surface areas (S_{BET}) were calculated from the isotherm analysis in the relative pressure range, where a linear BET plot with positive C constant was obtained. The total pore volumes were calculated at $P/P_0 = 0.95$. The transmission electron microscopy (TEM) images were obtained using a Jeol JEM 1230 operated at 120 kV. X-ray photoelectron spectroscopy (XPS) was performed on a Kratos Axis Ultra spectrometer using a monochromatic Al Kα source operating at 300 W. The survey and high-resolution spectra were acquired at pass energies of 160 eV and 20/40 eV, respectively. The electrical conductivity of the electrocatalysts (σ) was measured at room temperature by impedance spectroscopy over the frequency range of 1–1,000,000 Hz with a voltage of 0.1 V using an SI 1260 impedance/gain-phase analyzer from Solartron (Farnborough, Hampshire, UK). The pyrolyzed sample (~50 mg) was compressed in a hollow glass cylinder (with an inner diameter of 6 mm) between two metal plungers at thrust pressure of 1.04 MPa. The electrical connections to the impedance analyzer are at the end of each of those pistons. The very small sample thickness l (cm) was measured with a caliper as a difference between plunger distance in empty and filled cell. The electrical conductivity was calculated using Eq. (1):

$$\sigma = \frac{l}{R \cdot A} \quad (1)$$

where R is the resistance (Ω) and A is the area of the plunger surface (cm^2). The dispersion of platinum on electrocatalyst samples was measured by hydrogen chemisorption using a RXM-100 multicatalyst testing and characterization system (Advanced Scientific Design Inc.). The first H_2 adsorption isotherm was measured at room temperature, followed by outgassing for 1 h prior to a second H_2 adsorption isotherm determination under the same conditions. The Pt content of the electrocatalysts was measured using atomic absorption spectroscopy. The analysis was carried out using a Perkin–Elmer 1100B atomic absorption spectrometer. The carbon component was first removed by dry-ashing the catalysts in air at 900 °C. The ash residue was then digested in aqua regia and the resultant solution was filtered and diluted with de-ionized water to the appropriate concentration.

2.4. Performance tests of membrane-electrode assemblies (MEAs)

The catalyst ink was prepared by ultrasonic blending of the electrocatalysts with Nafion® solution (5 wt%, Sigma–Aldrich) in isopropyl alcohol for 2 h. To create the anode or cathode, this ink was then applied to the commercial gas diffusion layer (GDL, BASF) by successive brushing until the Pt loading of ~0.5 mg cm^{-2} was reached. The Nafion® content in the dry electrocatalyst was maintained at ca. 20 wt%. A commercially available gas-diffusion electrode (GDE, BASF, 0.5 mg_{Pt} cm^{-2}) was used at the other side without any further processing. The cathode and anode were applied to a Nafion®NRE-212 membrane to fabricate the membrane-electrode assembly (MEA). The geometric active area of the MEA was 2 cm^2. Fuel cell testing was carried out in a single cell. Hydrogen and air, humidified at 80 °C, were supplied to the anode and cathode at flow rates of 120 and 250 mL min^{-1}, respectively. Both electrodes were maintained at the same backpressure of 30 psig. Polarization experiments were conducted using a test station (Fideris™ Hydrogen Test Kit™) at cell temperature of 80 °C.

3. Results and discussion

3.1. Characteristic properties

In MOF-253, one-dimensional chains of hydroxide-bridged, octahedrally coordinated Al^{3+} cations are linked via $bpydc^{2-}$ ligands to give a three-dimensional framework with rhombic channels (Fig. 2) [35]. According to the previous observations upon insertion within the framework, the Pt atom is expected to fit the usual square planar geometry, with two Cl^- ions and two N atoms from bpydc [35].

As shown in Fig. 3a, XRD pattern of Pt-MOF exhibits similar diffraction peaks to that of the synthesized MOF-253 (and the previously reported Pd-MOF [35]), confirming that the MOF-253 structure is retained. To produce the PEMFC electrocatalysts, the Pt-MOF was pyrolyzed under flow of Ar atmosphere to form Pt nanoparticles. In was also expected that during pyrolysis the organic part of the synthesized Pt-MOFs would be carbonized to produce carbon, which provides the required electronic conductivity. In order to study the effect of pyrolysis temperature, the Pt-MOF was pyrolyzed at 700, 800, 950, and 1050 °C. The evidence for

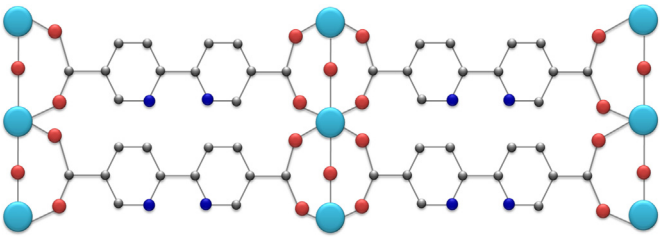

Fig. 2. (001) View of MOF-253 crystal.

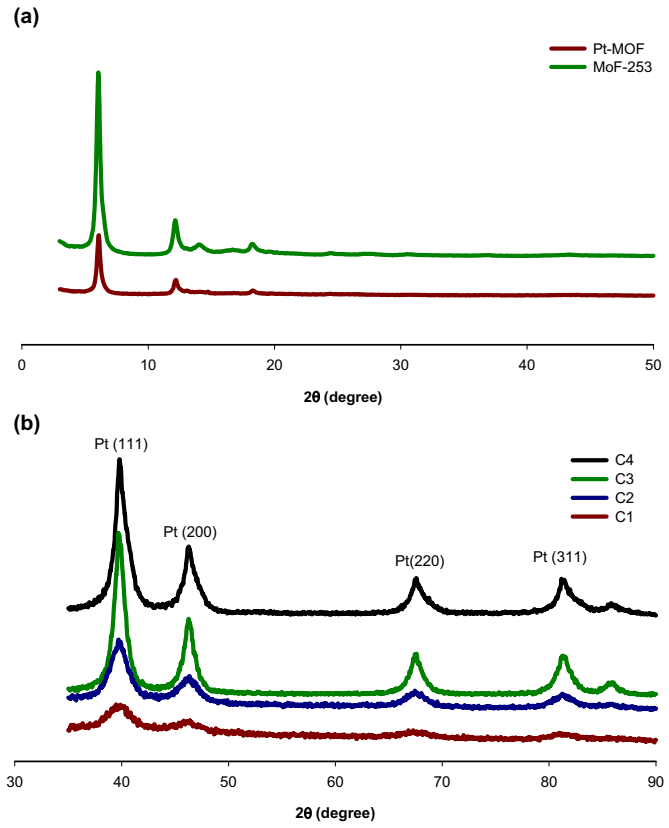

Fig. 3. XRD patterns of (a) MOF-253 and Pt-MOF, (b) carbonized C_1–C_4 samples.

the formation of Pt nanoparticles was clearly verified by XRD analysis. Fig. 3b shows the XRD patterns of the four carbonized Pt-MOF samples (C_1–C_4). In all cases, the diffraction peaks observed at around $2\theta = 40°$, 46°, 68°, and 81° were attributed to Pt (111), (200), (220), and (311) crystalline planes, respectively, representing typical crystalline Pt face-centered cubic (fcc) structure. It can also be seen from Fig. 3b that Al although present in high content is not XRD visible. In addition, the XRD patterns did not show any trace of Pt oxide phases.

For these samples, the diffraction peaks are indeed broad, confirming the formation of small Pt crystal domains. The average Pt crystal domain sizes were calculated from the Pt (220) reflection using Scherrer equation. Table 1 shows that the Pt crystal domain sizes in the carbonized samples were between 7 and 10 nm. With increasing carbonization temperature, the Pt crystal domain sizes first increased and then decreased. This most probably reflects the competition of two simultaneous processes occurring during the pyrolytic transformation of the Pt-MOF: 1) the formation of germinal Pt nanoparticles, 2) the coalescence of these nanoparticles to form larger Pt particles. As can be seen from Table 1, the minimum Pt crystal domain size was found for the sample carbonized at 800 °C (C_2), confirming the initial nanoparticle formation. At higher temperatures the coalescence of Pt crystal domains prevailed over formation of the initial Pt nanoparticles giving rise to bigger average crystal domain size.

Table 1
Average Pt particle size of the carbonized C_1–C_4 samples.

Electrocatalyst	Platinum average particle size (nm)
C_1	7.8
C_2	7.4
C_3	7.7
C_4	9.2

Nitrogen adsorption–desorption isotherms of the MOF-253 and Pt-MOF (see Fig. 4a) reveal a type I adsorption isotherm characteristic of a microporous solid. Table 2 shows reduced BET specific surface area and pore volume of the Pt-MOF compared to those of the MOF-253. The shape of isotherms of the carbonized Pt-MOF indicates the existence of both micropores and mesopores (see Fig. 4b). The steep increase at low relative pressure demonstrates the presence of micropores. The type IV isotherm with a capillary condensation step and a hysteresis loop near relative pressure (P/P_0) of ~0.5 in the desorption branch indicates the presence of mesopores. The pore size distributions were determined by using NLDFT method considering sorption of N_2 at −196 °C in slit/cylindrical carbon pores. The kernel of equilibrium NLDFT isotherms (desorption branch) was applied for pore width determination. As can be seen from the inset of Fig. 4b, the majority of pores are located in the mesopore region. This mesopore size corresponded to that of nanoporous carbon formed by carbonization of Pt-MOF. The presence of micropores (~10 Å equal to that of Pt-MOF) is reminiscent of the MOF structure. All samples display similar pore size distribution with a peak centered at ca. 5.0 nm, except for sample C_2 which shows an additional mode centered at 7.5 nm. As can be seen in Table 2, the specific surface areas and pore volumes did not vary too much with calcination temperature indicating evidently a minor restructuration of the carbon support above

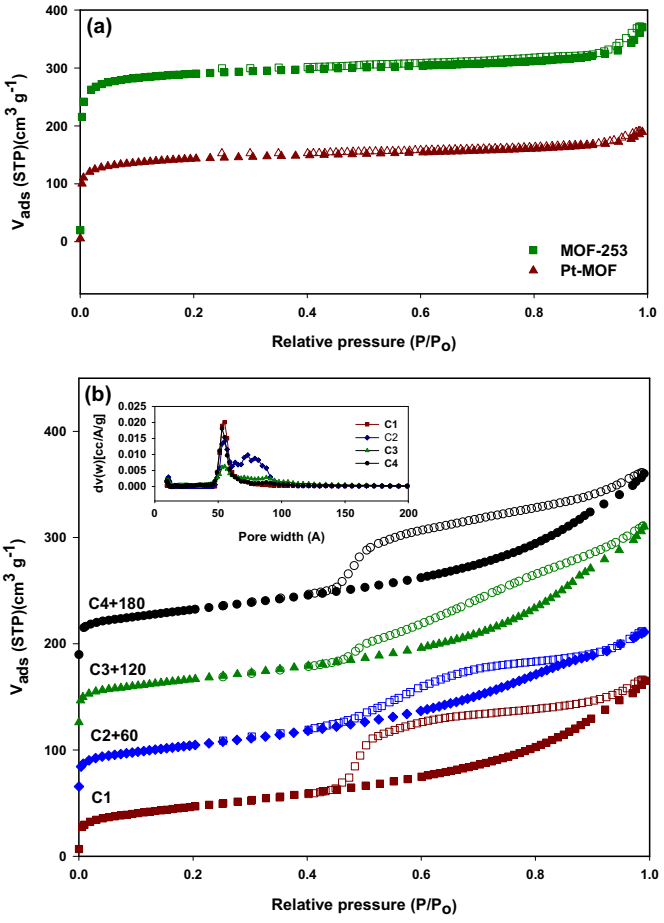

Fig. 4. N_2 adsorption–desorption isotherms of (a) MOF-253 and Pt-MOF, (b) carbonized C_1–C_4 samples (closed: adsorption; open: desorption).

Table 2
BET specific surface areas and pore volumes of the MOF materials and carbonized C_1–C_4 samples.

	S_{BET} m^2 gr^{-1}	V_{pore} cm^3 gr^{-1}
MOF-253	1155	0.51
Pt-MOF	540	0.27
C_1	165	0.23
C_2	160	0.22
C_3	165	0.26
C_4	185	0.25

700 °C. However, the platinum phase was affected by calcination more strongly, according to the following results.

TEM images (Fig. 5) of the carbonized Pt-MOFs reveal that all C_1–C_4 samples were amorphous carbon with a "foam-like" porous texture with embedded dark spherically shaped Pt nanoparticles. Fig. 5 shows that the size distribution of Pt particles is temperature dependent. The calculated average particle diameters are 3.5, 5.0, 6.2 and 7.2 for C_1, C_2, C_3 and C_4, respectively. TEM analysis of the electrocatalysts shows agreement with rough XRD evaluation of Pt crystal domain sizes (Table 1).

X-Ray photoelectron spectroscopy (XPS) was used to characterize the nature of platinum and carbon species of the prepared electrocatalysts, as exemplified by the results obtained from the C_1 and C_4 samples (carbonized respectively at the minimal and maximal temperatures in this study). The Pt 4*f* XPS spectrum of C_1 (Fig. 6a) could be deconvoluted into two pairs of doublets with weak peaks centered at binding energies of 71.2 and 74.6 eV, respectively. These two peaks are attributed to Pt $4f_{7/2}$ and Pt $4f_{5/2}$ excitations of metallic platinum, whereas the other intense peaks at 72.3 and 75.6 eV are due to oxidized platinum. In contrast for C_4, the Pt XPS spectrum (Fig. 6b) demonstrates only one pair of doublet with intense peaks centered at binding energies of 71.4 and 74.7 eV, respectively. These results indicate that a substantial amount of Pt was reduced to metallic Pt(0) during pyrolysis at higher temperatures. The C 1s XPS spectrum of the C_1 and C_4 samples (Fig. 6(c, d), respectively) consist of a peak at ca. 284.6 eV, which could be attributed to the sp^2 graphitic carbon species. For C_4, this peak has a full-width at half-maximum (FWHM) linewidth of 0.92 eV, close to that of the graphitized carbon black (0.82 eV) [36–38], revealing a well-ordered packing of graphene layers. However, in the case of C_1, this peak is broader with (FWHM) linewidth of 1.52 eV, suggesting the presence of less ordered graphene layers compared to the graphitized carbon black. In addition, N 1s XPS experiments showed the presence of pyridinic and pyrrolic N in these samples (Fig. 6e, f).

The results of complex impedance spectroscopy experiments carried out at room temperature are shown in Fig. 7. A plateau on Re (*Z*) versus frequency plot is observed at frequencies below 10–100 kHz for all four samples. The absence of electrode effects and diffusion phenomena at low frequencies definitely evidences existence of an electronic component in the conductivity of all four samples. It can be seen that the resistance of the electrocatalysts decreased with calcination temperature from 320 Ω to 1.8 Ω with corresponding rise of conductivity from 0.0024 S cm^{-1} to 0.4 S cm^{-1}.

As can be seen in Fig. 7a, the less conductive samples C_1 and C_2 demonstrates resistance decrease at higher frequencies (>100 kHz), which most probably can be attributed to the existence of an ionic conductance in these samples along with electronic component. In the same frequency range (>100 kHz), the resistance values are raised above the plateaux for samples C_3 and C_4 (Fig. 7b), which can be ascribed to inductive distortions of the

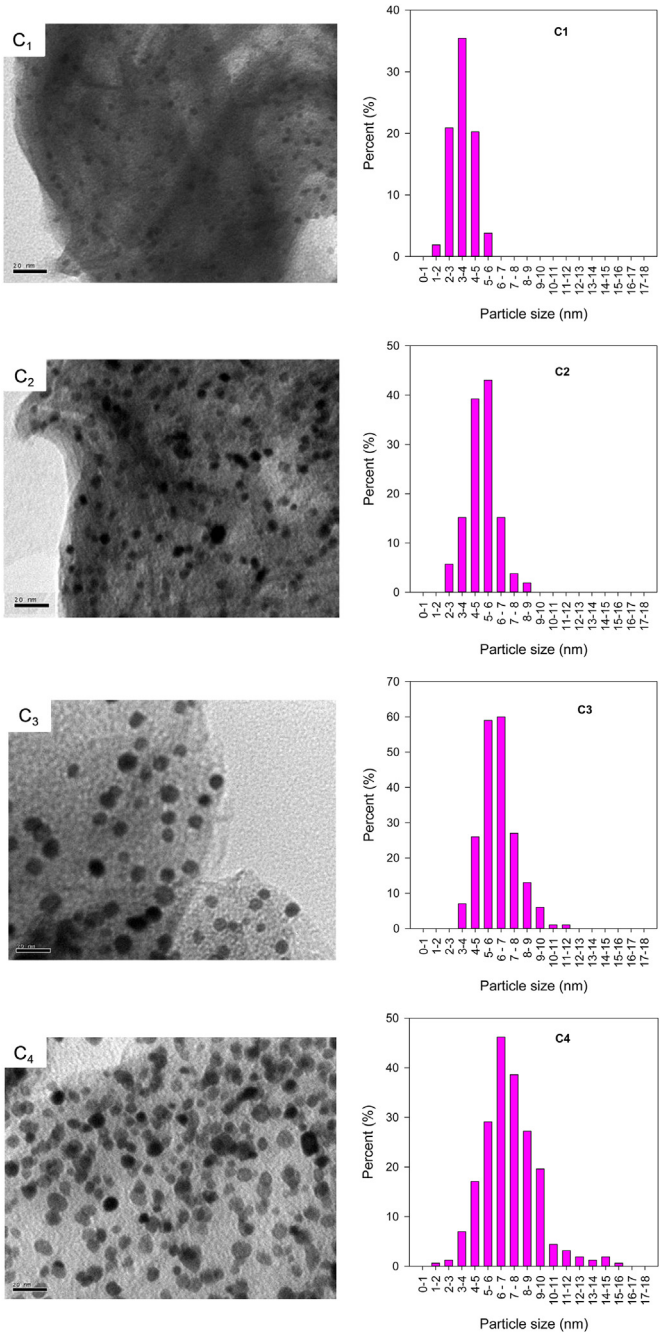

Fig. 5. TEM images and their corresponding histograms of particle size distribution of C_1–C_4 (the length of the bar in each photograph is 20 nm).

impedance response, accompanied by positive values of Im (*Z*) (Nyquist plot is not shown). It must be noted that these two samples show purely electronic conductance.

The origin of electronic conductivity in the pyrolyzed MOFs is obviously related to the graphitized carbon and partially to metallic Pt as follows from the results of XPS analysis. The conductivity of C_4 sample was found to be 0.4 S cm^{-1}, which is only one order of the magnitude lower than that of Vulcan XC-72 (4 S cm^{-1}) [39].

In Table 3, the values of Pt dispersion obtained from the hydrogen chemisorption isotherms are summarized. The C_1 and C_2 electrocatalysts carbonized at relatively lower temperatures exhibit slightly better dispersion compared to C_3 and C_4 samples. The

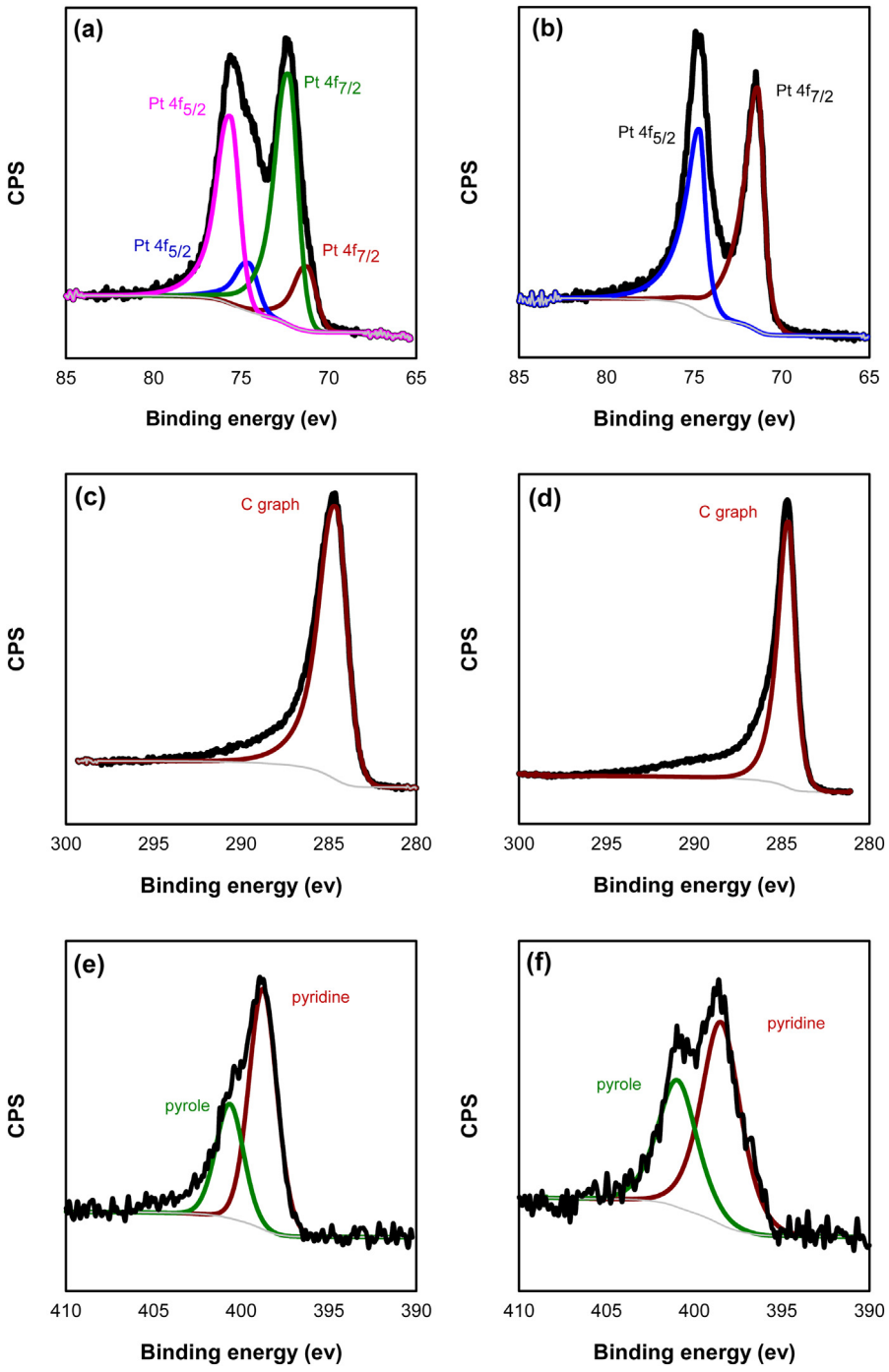

Fig. 6. Pt 4f XPS spectra of (a) C_1 and (b) C_4, C 1s XPS spectra of (c) C_1 and (d) C_4, and N 1s XPS spectra of (e) C_1 and (f) C_4.

average size of the Pt particles (d) can be obtained from the dispersion (N_S/N_T) resorting to the equation developed by van der Klink [40]:

$$N_T = \frac{2\pi}{3}\left(\frac{d}{a}\right)^3 \quad (2)$$

$$N_T = (10/3)l^3 - 5l^2 + (11/3)l - 1 \quad (3)$$

$$N_S = 10l^2 - 20l + 12 \quad (4)$$

where N_T is the total number of atoms, N_S is the number of surface atoms, l is the number of atomic layers, and a is the lattice parameter, which is equal to 0.392 nm for Pt. It can be observed in Table 3 that, the Pt dispersion values of all electrocatalysts correlate with the Pt particle sizes determined by XRD.

3.2. Single cell polarization test

Since only samples C_3 and C_4 showed a pure electronic conductivity of a few S cm^{-1}, these two samples were tested in a fuel cell. The primary investigation showed that the presence of Al in these electrocatalysts reduce their catalytic performance in the

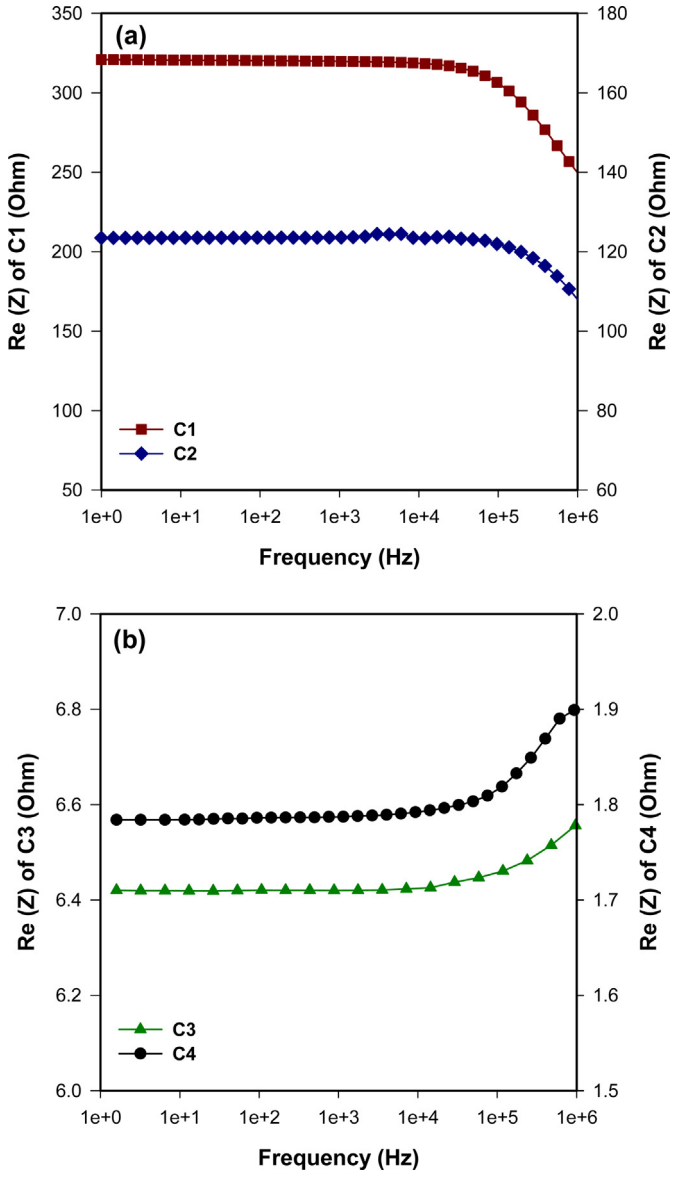

Fig. 7. Re (Z) vs. frequency for (a) C_1 and C_2 (b) C_3 and C_4 samples.

fuel cell, therefore, these samples were base-leached in 5 wt% NaOH solution at 70 °C for 6 h to remove inactive Al species from the electrocatalysts, and then thoroughly washed in de-ionized water until neutral pH. XRD patterns and TEM images showed no changes in Pt particle size upon this leaching step. Single-cell performance of the MEAs made with C_3 and C_4 electrocatalysts as the anode and a commercial electrode (BASF, 0.5 mg_{Pt} cm^{-2}) as the cathode is shown in Fig. 8. For comparison, the single-cell performance of the MEA made with commercial electrode for

Table 3
Pt dispersion and average particle size of carbonized C_1–C_4 samples determined by H_2 chemisorption.

	Dispersion %	Pt average particle size (d) nm
C_1	24	5.3
C_2	29	4.2
C_3	22	5.8
C_4	20	6.1

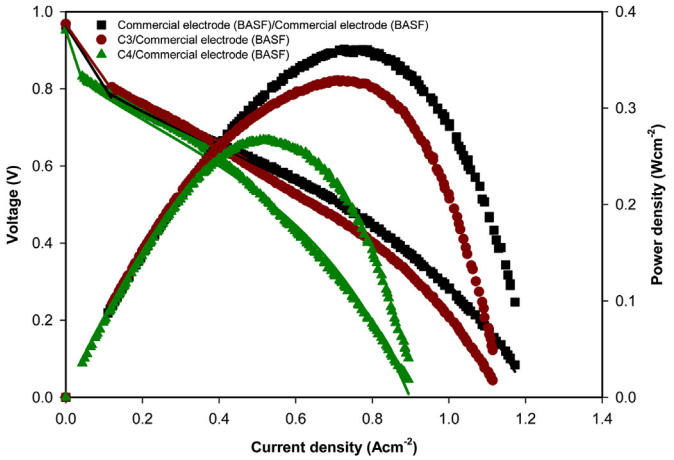

Fig. 8. Polarization and power curves of PEMFCs with anode: commercial (BASF) electrode, C_3 and C_4 based electrode, cathode: commercial (BASF) electrode. Polymer electrolyte membrane: Nafion®NRE-212. Pt loading on both the cathode and the anode: 0.5 mg cm^{-2}, Test conditions: cell temperature at 80 °C, H_2 and air flow rate of 120 and 250 mL min^{-1}, respectively, and 100% humidified gases at 30 psig. (solid lines are based on Eq. (5)).

both anode and cathode is also included. The Pt loading was maintained at 0.5 mg cm^{-2} on each electrode. The anode fabricated from C_3 electrocatalyst showed an open circuit voltage (OCV) of ~970 mV almost equal to the OCV of commercial electrode (~960 mV). However, in the case of anode made of C_4 electrocatalyst the OCV was somewhat smaller (~950 mV). Fig. 8 demonstrates that the anode prepared using C_3 electrocatalyst shows very similar power and polarization curves to the commercial electrode, especially in the kinetic range (low-current density). At a fixed cell voltage of 0.6 V, the current density of this electrode is 482 mA cm^{-2}, which is comparable to the commercial electrode (537 mA cm^{-2}). However, for the anode fabricated from C_4 electrocatalyst, the current density is 427 mA cm^{-2}, which is 20% smaller than that of the commercial electrode. The corresponding power densities normalized on the basis of Pt loading were 0.58 W mg_{Pt}^{-1} (C_3 based anode), 0.51 W mg_{Pt}^{-1} (C_4 based anode) and 0.64 W mg_{Pt}^{-1} (commercial electrode) at 0.6 V. Unlike the anode side, the performance of the cathode electrode (Fig. 9)

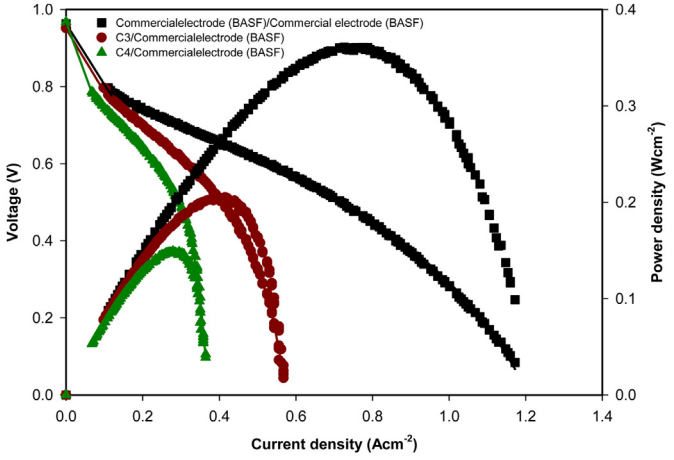

Fig. 9. Polarization and power curves of PEMFCs with anode: commercial (BASF) electrode, cathode: commercial (BASF) electrode, C_3 and C_4 based electrode. Polymer electrolyte membrane: Nafion®NRE-212. Pt loading on both the cathode and the anode: 0.5 mg cm^{-2}, Test conditions: cell temperature at 80 °C, H_2 and air flow rate of 120 and 250 mL min^{-1}, respectively, and 100% humidified gases at 30 psig. (solid lines are based on Eq. (5)).

Table 4
Electrochemical parameters of the resulting MEAs for oxygen reduction reaction.

MEA		E^0 (V)	b (V dec^{-1})	R (Ω cm^2)	m (V)	n (cm^2 A^{-1})	R^2
Anode	Cathode						
Commercial (BASF)	Commercial (BASF)	0.772	0.062	0.354	1.09E-03	4.75	0.9984
Commercial (BASF)	Prepared from C_3	0.799	0.060	0.714	6.63E-05	15.15	0.9993
Commercial (BASF)	Prepared from C_4	0.778	0.056	0.864	5.96E-06	30.47	0.9976
Commercial (BASF)	Commercial (BASF)	0.772	0.062	0.354	1.09E-03	4.75	0.9984
Prepared from C_3	Commercial (BASF)	0.798	0.058	0.389	3.93E-03	3.93	0.9993
Prepared from C_4	Commercial (BASF)	0.787	0.045	0.397	7.66E-03	4.49	0.9947

prepared from C_3 deviates from the commercial electrode. This deviation is again more pronounced in the case of cathode fabricated from C_4. At a fixed cell voltage of 0.6 V, the current density of the cathode prepared from C_3 and C_4 electrocatalysts were found to be 317 and 234 mA cm^{-2}, respectively, which is 40 and 56% smaller than that of the commercial electrode (537 mA cm^{-2}). The corresponding power densities normalized on the basis of Pt loading were 0.38 W mg_{Pt}^{-1} (C_3 based cathode), 0.28 W mg_{Pt}^{-1} (C_4 based cathode) and 0.64 W mg_{Pt}^{-1} (commercial electrode) at 0.6 V.

In order to obtain more detailed information about the electrode kinetic parameters for the oxygen reduction on these electrodes, the experimental polarization data were fitted to the following empirical equations [41]:

$$E = E^0 - b\log i - Ri - m\exp^{ni} \quad (5)$$

$$E^0 = E_r + b\log i^0 \quad (6)$$

where E (V) and i (A) are experimentally measured cell voltage and current, E_r (V) is the reversible cell voltage, i^0 (A) and b (V dec^{-1}) are the exchange current and the Tafel slope for oxygen reduction, respectively. R (Ω cm^2) represents the total DC resistance, which is a summation of resistances in the polymer membrane and other electrode components accountable for the linear part of the variation of potential with current. In particular, the two parameters m (V) and n (cm^2 A^{-1}) mean mass transport phenomena in PEMFC. The electrical cell potential linearly depends on parameter m, while it correlates with parameter n exponentially. Knowing m and n, mass transfer overpotential in the high current density region of the I–V curve, where the cell potential decreases exponentially because of mass transport limitation, can be estimated. The experimental data were fitted to Eqs. (5) and (6) using Matlab®'s curve fitting tool. The fitting method used was nonlinear least square and the algorithm used was trust-region approach. The kinetic parameters of these electrocatalysts are summarized in Table 4. The two electrocatalysts have similar b values of ca. 0.06 V, which is common to most supported and unsupported Pt electrodes [42]. However, the internal and mass transfer resistances of the cell were found to be larger when C_3 and C_4 samples were used as the electrocatalyst at the cathode electrode compared to the commercial cathode. This might be caused by either a) the intrinsic properties of the synthesized electrocatalysts, mainly conductivity and pore structure, which are dominated by calcination conditions; or b) the properties of the catalyst layer determined by its preparation method and the ink composition. The ink solution is prepared by mixing carbon supported platinum nanoparticles, with an aqueous solution of perfluorosulfonic acid polymer and isopropyl alcohol, which serves as a binder and proton conductor. The structural distribution of the resulting mixture determines the effective Pt surface area of the catalyst ink. In order to discover which of these sources have the main impact on fuel cell performance, the same analysis, using Eqs. (5) and (6), was done when C_3 and C_4 electrocatalysts are used at the anode side, and the results are summarized in Table 4. The contribution of internal resistance and mass transfer losses to the overall fuel cell performance is quite comparable to the commercial electrode, where the C_3 and C_4 based electrodes are placed at the anode side. Therefore, larger internal and mass transfer resistances of the cell with cathode electrodes prepared from C_3 and C_4 electrocatalysts is mainly related to the catalyst layer properties. The impact of structure and composition of a catalyst layer on overall PEMFCs performances have been clarified both by experimental and theoretical means. Many experimental studies were focused on optimization of cell performance as a function of Nafion content [43,44]. Here, both the cathode and anode catalyst layers were prepared from the same ink solution, which seems to be quite efficient at the anode side but needed to be modified for the cathode side.

4. Conclusion

An effective new approach toward preparing PEMFCs electrocatalysts was reported in which Pt containing MOF material was applied as the only precursor. Pt nanoparticles (7–10 nm) were produced by simple pyrolytic carbonization of Pt loaded MOF under flow of Ar. The electrocatalytic activities were tested in a single stack PEMFC. The results show that this rather simple technique allows producing electrocatalysts with performances comparable to the commercial materials. This new approach to preparing electrocatalysts is however prone to further improvement. In our work an inert atmosphere was used during MOF carbonization. Changing this atmosphere to a reactive gas such as ethylene or acetylene may allow better preserving the original atomic dispersion of Pt in the MOF. Moreover starting with MOF containing other metals such as Fe or Co can address the most challenging issue of employing non-PGM ORR catalysts owing to their relatively low turn-over-frequency in comparison with Pt. The Fe or Co containing MOF precursors could also provide the highest possible volumetric density of evenly distributed active sites and so may lead to a simple, original method to synthesize new electrocatalysts [32–34].

Acknowledgments

The authors would like to thank the Fonds Quebecois de Recherche sur la Nature et les Technologies (FQRNT) for financial support. The authors gratefully acknowledge the helpful comments by Prof. Jean-Pol Dodelet.

References

[1] C. Song, Catal. Today 77 (2002) 17–49.
[2] H. Gregor, Fuel Cell Technology Handbook, CRC Press, Birkenfeld, 2002.
[3] H.A. Gasteiger, S.S. Kocha, B. Sompalli, F.T. Wagner, Appl. Catal. B-Environ. 56 (2005) 9–35.

[4] B.D. James, J.A. Kalinoski, Mass Production Cost Estimation for Direct H_2 PEM Fuel Cell Systems for Automotive Applications, Virginia, Arlington, 2008. http://www.hydrogen.energy.gov/pdfs/review08/fc_7_james.pdf.
[5] K. Gong, F. Du, Z. Xia, M. Durstock, L. Dai, Science 323 (2009) 760–764.
[6] Y. Wang, Y. Shao, D.W. Matson, J. Li, Y. Lin, ACS Nano 4 (2010) 1790–1798.
[7] B. Winther-Jensen, O. Winther-Jensen, M. Forsyth, D.R. MacFarlane, Science 321 (2008) 671–674.
[8] Y. Li, Q. Liu, W. Shen, Dalton Trans. 40 (2011) 5811–5826.
[9] A. Stein, Z. Wang, M.A. Fierke, Adv. Mater. 21 (2009) 265–293.
[10] Y. Xia, Y. Xiong, B. Lim, S.E. Skrabalak, Angew. Chem. Int. Ed. 48 (2009) 60–103.
[11] C. Liu, C.-C. Wang, C.-C. Kei, Y.-C. Hsueh, T.-P. Perng, Small 5 (2009) 1535–1538.
[12] S. Litster, G. McLean, J. Power Sources 130 (2004) 61–76.
[13] J.R. Long, O.M. Yaghi, Chem. Soc. Rev. 38 (2009) 1213–1214.
[14] H.-C. Zhou, J.R. Long, O.M. Yaghi, Chem. Rev. 112 (2012) 673–674.
[15] S. Ma, D. Sun, M. Ambrogio, J.A. Fillinger, S. Parkin, H.-C. Zhou, J. Am. Chem. Soc. 129 (2007) 1858–1859.
[16] B. Wang, A.P. Cote, H. Furukawa, M. O'Keeffe, O.M. Yaghi, Nature 453 (2008) 207–211.
[17] M. Park, D. Moon, J.W. Yoon, J.-S. Chang, M.S. Lah, Chem. Commun. 45 (2009) 2026–2028.
[18] S. Ma, X.-S. Wang, D. Yuan, H.-C. Zhou, Angew. Chem. Int. Ed. 47 (2008) 4130–4133.
[19] B. Chen, S. Ma, F. Zapata, F.R. Fronczek, E.B. Lobkovsky, H.-C. Zhou, Inorg. Chem. 46 (2007) 1233–1236.
[20] S. Bourrelly, P.L. Llewellyn, C. Serre, F. Millange, T. Loiseau, G. Férey, J. Am. Chem. Soc. 127 (2005) 13519–13521.
[21] O.G. Nik, X.Y. Chen, S. Kaliaguine, J. Membr. Sci. 413-414 (2012) 48–61.
[22] H. Vinh-Thang, S. Kaliaguine, in: O.L. Ortiz, L.D. Ramírez (Eds.), Coordination Polymers and Metal Organic Frameworks: Properties, Types and Applications, Chemical Engineering Methods and Technology Series, Nova Science Publishers, Hauppauge, N.Y, 2011, pp. 129–168. (Chapter 4).
[23] P. Horcajada, T. Chalati, C. Serre, B. Gillet, C. Sebrie, T. Baati, J.F. Eubank, D. Heurtaux, P. Clayette, C. Kreuz, J.-S. Chang, Y.K. Hwang, V. Marsaud, P.-N. Bories, L. Cynober, S. Gil, G. Férey, P. Couvreur, R. Gref, Nat. Mater. 9 (2010) 172–178.
[24] P. Horcajada, C. Serre, G. Maurin, N.A. Ramsahye, F. Balas, M. Vallet-Regí, M. Sebban, F. Taulelle, G. Férey, J. Am. Chem. Soc. 130 (2008) 6774–6780.
[25] W.J. Rieter, K.M. Pott, K.M.L. Taylor, W. Lin, J. Am. Chem. Soc. 130 (2008) 11584–11585.
[26] C. Zlotea, R. Campesi, F. Cuevas, E. Leroy, P. Dibandjo, C. Volkringer, T. Loiseau, G. Ferey, M. Latroche, J. Am. Chem. Soc. 132 (2010) 2991–2997.
[27] D. Dybtsev, C. Serre, B. Schmitz, B. Panella, M. Hirscher, M. Latroche, P.L. Llewellyn, S. Cordier, Y. Molard, M. Haouas, F. Taulelle, G. Ferey, Langmuir 26 (2010) 11283–11290.
[28] K.K. Tanabe, S.M. Cohen, Chem. Soc. Rev. 40 (2011) 498–519.
[29] B. Liu, H. Shioyama, T. Akita, Q. Xu, J. Am. Chem. Soc. 130 (2008) 5390–5391.
[30] B. Liu, H. Shioyama, H. Jiang, X. Zhang, Q. Xu, Carbon 48 (2010) 456–463.
[31] J. Hu, H. Wang, Q. Gao, H. Guo, Carbon 48 (2010) 3599–3606.
[32] S. Ma, G.A. Goenaga, A.V. Call, D.-J. Liu, Chem. Eur. J. 17 (2011) 2063–2067.
[33] E. Proietti, F. Jaouen, M. Lefèvre, N. Larouche, J. Tian, J. Herranz, J.-P. Dodelet, Nat. Commun. 2 (2011) 416.
[34] D. Zhao, J.-L. Shui, C. Chen, X. Chen, B.M. Reprogle, D. Wang, D.-J. Liu, Chem. Sci. 3 (2012) 3200–3205.
[35] E.D. Bloch, D. Britt, C. Lee, C.J. Doonan, F.J. Uribe-Romo, H. Furukawa, J.R. Long, O.M. Yaghi, J. Am. Chem. Soc. 132 (2010) 14382–14384.
[36] H. Darmstadt, C. Roy, S. Kaliaguine, S.J. Choi, R. Ryoo, Carbon 40 (2002) 2673–2683.
[37] H. Darmstadt, C. Roy, S. Kaliaguine, T.-W. Kim, R. Ryoo, Chem. Mater. 15 (2003) 3300–3307.
[38] B. Sakintuna, Y. Yürüm, Ind. Eng. Chem. Res. 44 (2005) 2893–2902.
[39] D. Pantea, H. Darmstadt, S. Kaliaguine, L. Sümmchen, C. Roy, Carbon 39 (2001) 1147–1158.
[40] J.J. Van Der Klink, Adv. Catal. 44 (1999) 1–117.
[41] J. Kim, S.M. Lee, S. Srinivasan, C.E. Chamberlin, J. Electrochem. Soc. 142 (1995) 2670–2674.
[42] A. Parthasarathy, S. Srinivasan, A.J. Appleby, J. Electroanal. Chem. 339 (1992) 101–121.
[43] G. Sasikumar, J.W. Ihm, H. Ryu, J. Power Sources 132 (2004) 11–17.
[44] Z. Qi, A. Kaufman, J. Power Sources 113 (2003) 37–43.